

Fairing of Discrete Planar Curves by Integrable Discrete Analogue of Euler's Elasticae

Sebastián Elías GRAIFF ZURITA

Graduate School of Mathematics Kyushu University
744 Motooka, Nishi-ku, Fukuoka 819-0935, Japan

Kenji KAJIWARA

Institute of Mathematics for Industry, Kyushu University
744 Motooka, Fukuoka 819-0395, Japan

Toshitomo SUZUKI

Department of Architecture, Mukogawa Woman's University
1-13 Tozaki-cho, Nishinomiya, Hyogo 663-8121

Abstract

We construct a method to fair a given discrete planar curve by using the integrable discrete analogue of Euler's elastica, which is a discrete version of the approximation algorithm presented by D. Brander, et al. We first give a brief review of the integrable discrete analogue of Euler's elastica proposed by A. I. Bobenko and Yu. B. Suris, then we present a detailed account of the fairing algorithm, and we apply this method to an architectural problem of characterizing the keylines of Japanese handmade pantiles.

Keywords: Euler's elastica, integrable systems, discrete curve, discrete differential geometry

1 Introduction

The Euler's elastica (elastic curve) is a class of planar curves characterized as the solutions to the variational problem of minimizing the elastic energy under a certain boundary condition. It has been regarded as one of the most important class of planar curves because it is endowed with rich mathematical structure: exact solutions, integrability, geometry of elliptic curves, and so on, while it serves as a simple but realistic model of thin inextensible elastic rod (see, for example, [19, 29]). Brander et al. [5] have proposed an algorithm to fair a given planar curve segment by an Euler's elastica, motivated mainly by the development of the robotic hot-blade cutting technology. In this work, motivated by a problem of architecture to characterize the keylines of Japanese handmade pantiles, where the curve data is obtained in the form of discrete point data, we aim to construct a fairing method of discrete planar curves by using the integrable discrete analogue of the Euler's elastica proposed by Bobenko and Suris [3], which is referred to as the *discrete elastica* in this paper.

This paper is organized as follows. We give a brief review of the Euler's elastica and the discrete elastica in Sections 2 and 3, collecting the information on variational formulations, exact solutions and continuum limits with proofs. We present a detailed account of the fairing of a given discrete planar curve by the discrete elastica in Section 4. Finally, application to the characterization of the keylines of Japanese handmade pantiles is discussed in Section 5. For various formulas of the Jacobi elliptic functions used in this paper, the readers may refer to [24], for example.

2 Euler's elastica

Let $\gamma(s) \in \mathbb{R}^2$ ($s \in \mathbb{R}$) be an arc length parameterized planar curve. By definition, it holds that $\|\gamma'(s)\| = 1$, where $' = \frac{d}{ds}$. The tangent and normal vectors are defined by $T(s) = \gamma'(s)$ and $N(s) = R(\pi/2)T(s)$, respectively, where

$$R(\varphi) = \begin{bmatrix} \cos \varphi & -\sin \varphi \\ \sin \varphi & \cos \varphi \end{bmatrix}. \quad (2.1)$$

Due to $\|\gamma'(s)\| = 1$, it is possible to parameterize the tangent vector as

$$T(s) = \begin{bmatrix} \cos \theta(s) \\ \sin \theta(s) \end{bmatrix}, \quad (2.2)$$

where the angle function $\theta(s)$ is the angle of $T(s)$ measured from the horizontal axis in the counterclockwise direction. Introducing the Frenet frame $\Phi(s)$ by

$$\Phi(s) = [T(s), N(s)] \in \text{SO}(2), \quad (2.3)$$

we have the Frenet formula,

$$\Phi'(s) = \Phi(s)L(s), \quad L(s) = \begin{bmatrix} 0 & -\kappa(s) \\ \kappa(s) & 0 \end{bmatrix}, \quad (2.4)$$

where $\kappa(s) = \theta'(s)$ is the (signed) curvature. The Euler's elastica (or simply referred to as the

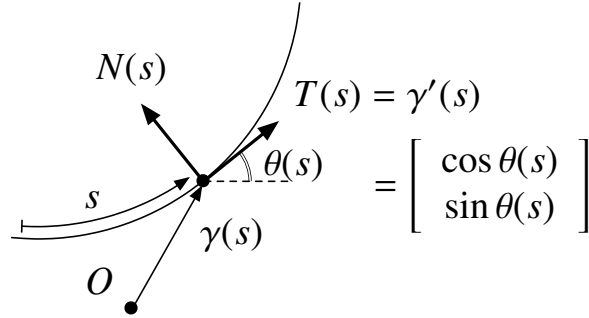


Figure 1: Smooth planar curve and the Frenet frame.

elastica) is defined as a critical point of the elastic energy

$$E = \int_0^L (\kappa(s))^2 ds, \quad (2.5)$$

with respect to variations with fixed endpoints and tangent vectors at the endpoints, under the condition of preserving the total length. The Euler-Lagrange equation yields the following differential equations for the curvature and the angle function:

Proposition 2.1. *The curvature κ of the Euler's elastica satisfies*

$$\kappa'' + \frac{1}{2}\kappa^3 - \lambda\kappa = 0, \quad (2.6)$$

where $\lambda \in \mathbb{R}$ is a constant. Moreover, the angle function θ satisfies

$$\theta'' + \mu \sin \theta = 0, \quad (2.7)$$

where $\mu > 0$ is a constant.

Derivation of equation (2.6) is given in various literatures such as [29]. Here, we show a concise derivation using the variation of the tangent vector. Consider the functional

$$S = \int_0^L \left(\langle T', T' \rangle + c \langle T, T \rangle + \langle a, T \rangle \right) ds, \quad (2.8)$$

where the first term is the elastic energy, and the second and third terms correspond to the preservation $\|T\|$ and $\gamma(L) - \gamma(0)$, respectively, with $c = c(s) \in \mathbb{R}$ and $a \in \mathbb{R}^2$ being the Lagrange multipliers. The variation of S is calculated by using the Frenet formula (2.4) as

$$\begin{aligned} \delta S &= \int_0^L \left(2 \langle T', \delta T' \rangle + 2c(s) \langle T, \delta T \rangle + \langle a, \delta T \rangle \right) ds \\ &= 2 \langle T', \delta T \rangle \Big|_0^L + 2 \int_0^L \left\langle (\kappa^2 + c(s))T - \kappa'N + \frac{a}{2}, \delta T \right\rangle ds. \end{aligned} \quad (2.9)$$

The first term is the boundary term that vanishes due to the boundary condition, and the second term gives the Euler-Lagrange equation,

$$(\kappa^2 + c)T - \kappa'N + \frac{a}{2} = 0. \quad (2.10)$$

Taking the scalar product with T and N , we have

$$\kappa^2 + c + \frac{1}{2} \langle a, T \rangle = 0 \quad \text{and} \quad -\kappa' + \frac{1}{2} \langle a, N \rangle = 0, \quad (2.11)$$

respectively. Multiplying κ' to both sides of the second equation of equation (2.11), we find that it is integrated to give

$$\frac{\kappa^2}{2} - \lambda = \frac{1}{2} \langle a, T \rangle, \quad (2.12)$$

where $\lambda \in \mathbb{R}$ is a constant of integration. Eliminating $\langle a, T \rangle$ from the first equation of (2.11) and equation (2.12), c is determined consistently as $c = -\frac{3}{2}\kappa^2 + \lambda$. Differentiating the second equation of equation (2.11) gives

$$\kappa'' = -\frac{\kappa}{2} \langle a, T \rangle. \quad (2.13)$$

Then eliminating $\langle a, T \rangle$ from equations (2.12) and (2.13) yields

$$\kappa'' + \kappa \left(\frac{\kappa^2}{2} - \lambda \right) = 0, \quad (2.14)$$

which is nothing but equation (2.6).

Remark 2.2.

- (1) Equation (2.6) is derived from equation (2.7) as follows. Multiplying θ' on both sides of equation (2.7), we see that equation (2.7) is integrated to give

$$\frac{1}{2}(\theta')^2 = \mu \cos \theta + \lambda, \quad (2.15)$$

where λ is a constant of integration. Then differentiating equation (2.7) and using equation (2.15) yields

$$\kappa'' = -\mu \cos \theta \times \theta' = \left(-\frac{1}{2}\kappa^2 + \lambda \right) \kappa, \quad (2.16)$$

which is nothing but equation (2.6).

- (2) Equations (2.6) and (2.7) can be seen as travelling-wave reductions of the (focusing) modified KdV equation

$$\frac{\partial \kappa}{\partial t} + \frac{3}{2}\kappa^2 \frac{\partial \kappa}{\partial s} + \frac{\partial^3 \kappa}{\partial s^3} = 0 \quad (2.17)$$

and the sine-Gordon equation,

$$\frac{\partial^2 \theta}{\partial s \partial y} = \sin \theta, \quad (2.18)$$

respectively, where the former describes the integrable deformation of planar curves [8, 13].

It is known that the differential equations (2.6) and (2.7) can be solved in terms of the Jacobi elliptic functions. This is well-known, but we present the solutions for the readers' convenience. In the literature, the solutions are often constructed from the the first integral of (2.6) given by

$$(\kappa')^2 + \frac{\kappa^4}{2} - \lambda \kappa^2 = C, \quad (2.19)$$

where C is a conserved quantity (constant). Here we present those solutions and verify them by the differential equations for the Jacobi elliptic functions.

Proposition 2.3. *The curvature κ and the angle function θ can be expressed in terms of the Jacobi elliptic functions as follows:*

(i)

$$\kappa = 2k^{-1}\sqrt{\mu} \operatorname{dn} \left(k^{-1}\sqrt{\mu}s; k \right), \quad (2.20)$$

$$\sin \frac{\theta}{2} = \operatorname{sn} \left(k^{-1}\sqrt{\mu}s; k \right), \quad \mu = \frac{\lambda}{2k^{-2} - 1}. \quad (2.21)$$

(ii)

$$\kappa = 2k\sqrt{\mu} \operatorname{cn} \left(\sqrt{\mu}s; k \right), \quad (2.22)$$

$$\sin \frac{\theta}{2} = k \operatorname{sn} \left(\sqrt{\mu}s; k \right), \quad \mu = \frac{\lambda}{2k^2 - 1}. \quad (2.23)$$

Proof. It can be easily verified that equations (2.20) and (2.22) satisfy equation (2.6) from the differential equations for the dn and cn functions [24]

$$y = \operatorname{dn}(x, k), \quad \frac{d^2 y}{dx^2} = (2 - k^2)y - 2y^3, \quad (2.24)$$

$$y = \operatorname{cn}(x, k), \quad \frac{d^2 y}{dx^2} = (2k^2 - 1)y - 2k^2 y^3, \quad (2.25)$$

respectively, by applying suitable scale transformations. Also, equations (2.21) and (2.23) are shown to satisfy equation (2.7) in a similar manner. \square

Remark 2.4. *The Jacobi elliptic functions can be extended to modules $k > 1$, see, for example, [17, 24]. Thus, there exists an analytic continuation for all Jacobi elliptic functions in the range $k \geq 0$. In this way, cases (i) and (ii) can be regarded as one. As it is known, the case (i) (resp. (ii)) yields the elastica without (resp. with) inflection points; see Figure 4.*

3 Integrable discrete Euler's elastica

3.1 Basic framework of discrete planar curves

We first introduce the basic framework for discrete planar curves [12, 14, 20]. Let $\gamma_n \in \mathbb{R}^2$ ($n \in \mathbb{Z}$) be a discrete planar curve with $|\gamma_{n+1} - \gamma_n| = h$, where $h > 0$ is a constant. We also assume $\det(\gamma_{n+1} - \gamma_n, \gamma_n - \gamma_{n-1}) \neq 0$, i.e., not three consecutive points are collinear. Then γ_n is called a discrete planar curve with segment length h . We define the discrete tangent and normal vectors by

$$T_n = \frac{\gamma_{n+1} - \gamma_n}{h} = \begin{bmatrix} \cos \Theta_n \\ \sin \Theta_n \end{bmatrix} \quad \text{and} \quad N_n = R\left(\frac{\pi}{2}\right)T_n, \quad (3.1)$$

respectively, where the discrete angle function Θ_n is the angle of T_n measured from the horizontal axis in the counterclockwise direction. The discrete Frenet frame is defined by

$$\Phi_n = [T_n, N_n] \in \operatorname{SO}(2), \quad (3.2)$$

and the discrete Frenet formula by

$$\Phi_{n+1} = \Phi_n L_n, \quad L_n = R(K_{n+1}), \quad (3.3)$$

where $K_n = \Theta_n - \Theta_{n-1}$ is the angle between two adjacent tangent vectors. Equation (3.3) is the discrete version of the Frenet formula (2.4); see Figure 2. The discrete curvature κ_n can be defined as the reciprocal of the radius ρ_n of the osculating circle touching two adjacent segments at their midpoints [12] (see Figure 3),

$$\kappa_n = \frac{1}{\rho_n} = \frac{2}{h} \tan \frac{K_n}{2}. \quad (3.4)$$

We note that the discrete Frenet formula (3.3) can be written in terms of κ_n as

$$\frac{\Phi_n - \Phi_{n-1}}{h} = \frac{\Phi_n + \Phi_{n-1}}{2} \begin{bmatrix} 0 & -\kappa_n \\ \kappa_n & 0 \end{bmatrix}. \quad (3.5)$$

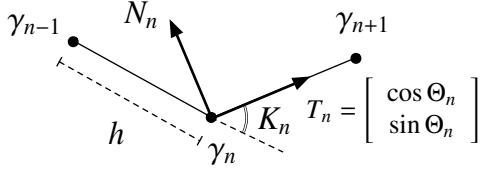


Figure 2: Discrete planar curve and the Frenet frame.

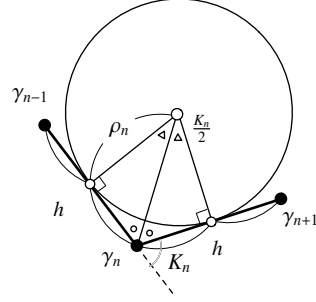


Figure 3: Discrete curvature of discrete arc length planar curve.

3.2 Discrete Euler's elastica

The discrete Euler's elastica [3, 4, 11] is defined as a discrete planar curve γ_n with segment length h that is a critical point of the functional

$$E_d = \sum_{n=1}^{N-1} \frac{2}{h} \log \left(1 + \frac{h^2}{4} \kappa_n^2 \right) \cong \sum_{n=1}^{N-1} \frac{2}{h} \log (1 + \langle T_{n-1}, T_n \rangle), \quad (3.6)$$

with respect to variation with fixed endpoints and end edges. Note that \cong means that the two functionals yield the same critical points. As mentioned in [4], E_d can be regarded as a discrete analogue of the elastic energy (2.5), in a sense that $2/h \log(1 + h^2 \kappa_n^2/4)$ is the potential energy of the bending force proportional to the discrete curvature κ_n at each vertex.

Taking into account the preservation of $\|\gamma_n - \gamma_{n-1}\|$ and $\gamma_N - \gamma_0$ by introducing the Lagrange multipliers $c_n \in \mathbb{R}$ and $a \in \mathbb{R}^2$, respectively, consider the functional

$$S_d = \sum_{n=1}^{N-1} \frac{2}{h} \log (1 + \langle T_{n-1}, T_n \rangle) + \sum_{n=0}^{N-1} (c_n \langle T_n, T_n \rangle + h \langle a, T_n \rangle). \quad (3.7)$$

Proposition 3.1. *The Euler-Lagrange equation for the functional (3.7) is given by*

$$\frac{2}{h} \frac{T_{n-1}}{1 + \langle T_{n-1}, T_n \rangle} + \frac{2}{h} \frac{T_{n+1}}{1 + \langle T_n, T_{n+1} \rangle} + 2c_n T_n + ha = 0, \quad (3.8)$$

or, equivalently, in terms of the discrete curvature κ_n by

$$\kappa_{n+1} + \kappa_{n-1} = \frac{\alpha \kappa_n}{1 + \frac{h^2}{4} \kappa_n^2}, \quad (3.9)$$

where $\alpha \in \mathbb{R}$ is a constant.

Proof. The variation of S_d is calculated as follows:

$$\begin{aligned} \delta S_d &= \sum_{n=1}^{N-1} \left(\frac{2}{h} \frac{\langle \delta T_{n-1}, T_n \rangle}{1 + \langle T_{n-1}, T_n \rangle} + \frac{2}{h} \frac{\langle T_{n-1}, \delta T_n \rangle}{1 + \langle T_{n-1}, T_n \rangle} \right) + \sum_{n=0}^{N-1} \left(2c_n \langle T_n, \delta T_n \rangle + h \langle a, \delta T_n \rangle \right) \\ &= R + \sum_{n=1}^{N-2} \left\langle \frac{2}{h} \frac{T_{n-1}}{1 + \langle T_{n-1}, T_n \rangle} + \frac{2}{h} \frac{T_{n+1}}{1 + \langle T_n, T_{n+1} \rangle} + 2c_n T_n + ha, \delta T_n \right\rangle, \end{aligned} \quad (3.10)$$

where R is the boundary term given by

$$R = \left\langle \frac{2}{h} \frac{T_1}{1 + \langle T_0, T_1 \rangle} + 2c_0 T_0 + ha, \delta T_0 \right\rangle + \left\langle \frac{2}{h} \frac{T_{N-2}}{1 + \langle T_{N-2}, T_{N-1} \rangle} + 2c_{N-1} T_{N-1} + ha, \delta T_{N-1} \right\rangle,$$

which vanishes due to the boundary condition. Setting $\delta S_d = 0$ gives the Euler-Lagrange equation,

$$\frac{2}{h} \frac{T_{n-1}}{1 + \langle T_{n-1}, T_n \rangle} + \frac{2}{h} \frac{T_{n+1}}{1 + \langle T_n, T_{n+1} \rangle} + 2c_n T_n + ha = 0, \quad (3.11)$$

which proves the first part. For the second part we use the discrete Frenet formula (3.5) written explicitly in terms of the tangent and normal vectors,

$$\frac{T_n - T_{n-1}}{h} = \kappa_n \frac{N_n + N_{n-1}}{2}, \quad \frac{N_n - N_{n-1}}{h} = -\kappa_n \frac{T_n + T_{n-1}}{2}. \quad (3.12)$$

From the discrete Frenet formula (3.3) and equation (3.4) we have that

$$\frac{2}{h} \frac{\langle T_{n-1}, N_n \rangle}{1 + \langle T_{n-1}, T_n \rangle} = -\kappa_n, \quad \frac{2}{h} \frac{\langle T_n, N_n \rangle}{1 + \langle T_n, T_{n+1} \rangle} = \kappa_{n+1}, \quad (3.13)$$

thus taking the inner product of both hand sides of equation (3.8) with N_n gives

$$\kappa_n - \kappa_{n+1} = h \langle a, N_n \rangle. \quad (3.14)$$

Then, taking the inner product of the first equation in the discrete Frenet formula (3.12) with a gives

$$\langle a, T_n \rangle - \langle a, T_{n-1} \rangle = -\frac{1}{2} \kappa_n \kappa_{n+1} + \frac{1}{2} \kappa_{n-1} \kappa_n, \quad (3.15)$$

which implies that exists a constant $\lambda \in \mathbb{R}$ such that

$$\langle a, T_n \rangle = -\frac{1}{2} \kappa_n \kappa_{n+1} + \lambda. \quad (3.16)$$

Finally taking the inner product of the second equation in the discrete Frenet formula (3.12) with a , and using equations (3.14) and (3.16), yields

$$(\kappa_{n+1} + \kappa_{n-1}) \left(1 + \frac{h^2}{4} \kappa_n^2 \right) = (2 + h^2 \lambda) \kappa_n, \quad (3.17)$$

which is exactly equation (3.9) with $\alpha = 2 + h^2 \lambda$. \square

By using a technique similar to the one shown in [31], we construct explicit solutions to equation (3.9) from its discrete first integral,

$$\kappa_{n+1}^2 + \kappa_n^2 - \alpha \kappa_{n+1} \kappa_n + \frac{h^2}{4} \kappa_{n+1}^2 \kappa_n^2 = C, \quad (3.18)$$

where $C \in \mathbb{R}$ is a constant (conserved quantity). Here, we avoid the long computation required and simply present the solutions corresponding to equations (2.20) and (2.22), and verify them by using the addition formulas for the Jacobi elliptic functions.

Proposition 3.2. Let $z \in \mathbb{R}$ be a constant. Then the following functions satisfy equation (3.9).

(i)

$$\begin{aligned}\kappa_n &= \frac{2 \operatorname{sn}(k^{-1}z; k)}{h \operatorname{cn}(k^{-1}z; k)} \operatorname{dn}(k^{-1}zn; k), \\ \alpha &= 2 \frac{\operatorname{dn}(k^{-1}z; k)}{\operatorname{cn}^2(k^{-1}z; k)}.\end{aligned}\tag{3.19}$$

(ii)

$$\begin{aligned}\kappa_n &= \frac{2k \operatorname{sn}(z; k)}{h \operatorname{dn}(z; k)} \operatorname{cn}(zn; k), \\ \alpha &= 2 \frac{\operatorname{cn}(z; k)}{\operatorname{dn}^2(z; k)}.\end{aligned}\tag{3.20}$$

Proof. These solutions are verified directly by the addition formulas for the dn and cn functions [24]. On the one hand, we use that

$$\operatorname{dn}(u+v) + \operatorname{dn}(u-v) = \frac{\frac{2 \operatorname{dn} v}{\operatorname{cn}^2 v} \operatorname{dn} u}{1 + \frac{\operatorname{sn}^2 v}{\operatorname{cn}^2 v} \operatorname{dn}^2 u}.\tag{3.21}$$

Putting $u = k^{-1}zn$, $v = k^{-1}z$ and $\kappa_n = a \operatorname{dn}(u; k)$, and comparing equation (3.21) with equation (3.9), we see that

$$\frac{1}{a^2} \frac{\operatorname{sn}^2 v}{\operatorname{cn}^2 v} = \frac{h^2}{4}, \quad \frac{2 \operatorname{dn} v}{\operatorname{cn}^2 v} = \alpha,\tag{3.22}$$

which proves (i). Similarly, on the other hand we use

$$\operatorname{cn}(u+v) + \operatorname{cn}(u-v) = \frac{\frac{2 \operatorname{cn} v}{\operatorname{dn}^2 v} \operatorname{cn} u}{1 + \frac{k^2 \operatorname{sn}^2 v}{\operatorname{dn}^2 v} \operatorname{cn}^2 u}.\tag{3.23}$$

Then putting $u = zn$, $v = z$ and $\kappa_n = b \operatorname{cn}(u; k)$, we get equation (3.9) with

$$\frac{1}{b^2} \frac{k^2 \operatorname{sn}^2 v}{\operatorname{dn}^2 v} = \frac{h^2}{4}, \quad \frac{2 \operatorname{cn} v}{\operatorname{dn}^2 v} = \alpha,\tag{3.24}$$

which proves (ii). □

Remark 3.3.

(1) Comparing equations (2.20) and (3.19), we see that there exists a constant Ω such that $\kappa_n = \kappa(\Omega n)$. Indeed, we have

$$\Omega = \frac{v}{\sqrt{\frac{\lambda}{2-k^2}}} \quad \text{and} \quad v = \operatorname{sn}^{-1} \sqrt{\frac{\frac{\lambda h^2}{2-k^2}}{1 + \frac{\lambda h^2}{2-k^2}}}.\tag{3.25}$$

There is also a similar relationship between equations (2.22) and (3.20). This implies that the discrete curvature κ_n is an “exact discretization” of the smooth curvature $\kappa(s)$.

(2) By putting $\alpha = h^2\lambda + 2$ and $nh = s$, equation (3.9) yields equation (2.6) in the continuum limit $h \rightarrow 0$. On the level of solutions, the following parametrizations of z ,

$$z = \begin{cases} \sqrt{\frac{\lambda}{2k^{-2} - 1}} h & \text{for (i),} \\ \sqrt{\frac{\lambda}{2k^2 - 1}} h & \text{for (ii),} \end{cases} \quad (3.26)$$

$$z = \begin{cases} \sqrt{\frac{\lambda}{2k^{-2} - 1}} h & \text{for (i),} \\ \sqrt{\frac{\lambda}{2k^2 - 1}} h & \text{for (ii),} \end{cases} \quad (3.27)$$

are consistent in the continuum limit to equations (2.21) and (2.23), respectively.

(3) Equation (3.9) is also known as the McMillan map, which is a special case of the Quispel-Roberts-Thompson (QRT) map solved by elliptic functions [26]. It can also be regarded as an autonomous version of a discrete Painlevé II equation [15, 16, 27]

(4) It is known that position vectors of both smooth and discrete elasticae admit explicit formulas in terms of the elliptic theta functions [21, 23].

Figure 4 illustrates typical examples of both smooth and discrete elasticae.

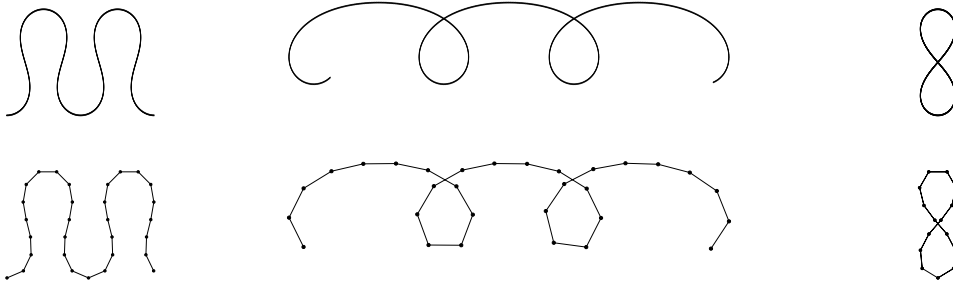


Figure 4: Typical examples of smooth and discrete elasticae. Left: (ii) $k = 0.8$, middle: (i) $k = 0.909$, right: (ii) $k = 0.9089 \dots$ (smooth), $k = 0.919 \dots$ (discrete).

3.3 Discrete Euler's elastica in terms of a potential function

Following [13], we say that θ_n is a *potential function* if it is such that

$$\Theta_n = \frac{\theta_{n+1} + \theta_n}{2}. \quad (3.28)$$

In this context, the discrete curvature is written as

$$\kappa_n = \frac{2}{h} \tan\left(\frac{\theta_{n+1} - \theta_{n-1}}{4}\right). \quad (3.29)$$

Proposition 3.4. *Suppose that θ_n satisfies*

$$\sin\left(\frac{\theta_{n+1} - 2\theta_n + \theta_{n-1}}{4}\right) + \epsilon \sin\left(\frac{\theta_{n+1} + 2\theta_n + \theta_{n-1}}{4}\right) = 0, \quad (3.30)$$

where $\epsilon \in \mathbb{R}$ is a constant. Then we have:

(1) It holds that

$$\cos\left(\frac{\theta_{n+1} - \theta_n}{2}\right) + \epsilon \cos\left(\frac{\theta_{n+1} + \theta_n}{2}\right) = \Lambda, \quad (3.31)$$

where $\Lambda \in \mathbb{R}$ is a constant.

(2) The discrete curvature satisfies equation (3.9) with $\alpha = 2(1 - \epsilon^2)/\Lambda^2$.

Proof. The first statement is shown as follows. Multiplying $\sin\left(\frac{\theta_{n+1} - \theta_{n-1}}{4}\right)$ to equation (3.30), using the product-to-sum formula, and rearranging terms gives:

$$\cos\left(\frac{\theta_{n+1} - \theta_n}{2}\right) + \epsilon \cos\left(\frac{\theta_{n+1} + \theta_n}{2}\right) = \cos\left(\frac{\theta_n - \theta_{n-1}}{2}\right) + \epsilon \cos\left(\frac{\theta_n + \theta_{n-1}}{2}\right), \quad (3.32)$$

which implies (3.31). In order to show the second statement, we introduce

$$\varphi_n = \frac{\theta_{n+1} - \theta_n}{2}, \quad \psi_n = \frac{\theta_{n+1} + \theta_n}{2}, \quad (3.33)$$

for simplicity in the notation. We have that $K_n = \psi_n - \psi_{n-1} = \varphi_n + \varphi_{n-1}$, and equation (3.30) is rewritten as

$$\sin\left(\frac{\varphi_n - \varphi_{n-1}}{2}\right) = -\epsilon \sin\left(\frac{\psi_n + \psi_{n-1}}{2}\right). \quad (3.34)$$

We expand equation (3.34) as

$$\sin \varphi_n \cos \frac{K_n}{2} - \cos \varphi_n \sin \frac{K_n}{2} = -\epsilon \sin \psi_n \cos \frac{K_n}{2} + \epsilon \cos \psi_n \sin \frac{K_n}{2}, \quad (3.35)$$

which gives

$$\tan \frac{K_n}{2} = \frac{\sin \varphi_n + \epsilon \sin \psi_n}{\Lambda} \quad \text{and} \quad \tan \frac{K_{n+1}}{2} = \frac{\sin \varphi_n - \epsilon \sin \psi_n}{\Lambda}, \quad (3.36)$$

where we used equation (3.31). From equation (3.36) and the sum-to-product formula, we have

$$\Lambda \left(\tan \frac{K_{n+1}}{2} + \tan \frac{K_{n-1}}{2} \right) = 2 \sin \frac{K_n}{2} \left[\cos \left(\frac{\varphi_n - \varphi_{n-1}}{2} \right) - \epsilon \cos \left(\frac{\psi_n + \psi_{n-1}}{2} \right) \right]. \quad (3.37)$$

We use the following two expressions: On the one hand, from equation (3.30),

$$\cos^2 \left(\frac{\varphi_n - \varphi_{n-1}}{2} \right) - \epsilon^2 \cos^2 \left(\frac{\psi_n + \psi_{n-1}}{2} \right) = 1 - \epsilon^2. \quad (3.38)$$

On the other hand,

$$\begin{aligned} \cos \left(\frac{\varphi_n - \varphi_{n-1}}{2} \right) + \epsilon \cos \left(\frac{\psi_n + \psi_{n-1}}{2} \right) &= \cos \frac{K_n}{2} (\cos \varphi_n + \epsilon \cos \psi_n) + \sin \frac{K_n}{2} (\sin \varphi_n + \epsilon \sin \psi_n) \\ &= \frac{\Lambda}{\cos \frac{K_n}{2}}, \end{aligned} \quad (3.39)$$

where we used equation (3.31) and (3.36). Finally, we multiply equation (3.37) by equation (3.39) to obtain

$$\Lambda \left(\tan \frac{K_{n+1}}{2} + \tan \frac{K_{n-1}}{2} \right) \text{prop} : \text{sogo} \frac{\Lambda}{\cos \frac{K_n}{2}} = 2 \sin \frac{K_n}{2} (1 - \epsilon^2), \quad (3.40)$$

where we used (3.38), which is rewritten as

$$\tan \frac{K_{n+1}}{2} + \tan \frac{K_{n-1}}{2} = \frac{1 - \epsilon^2}{\Lambda^2} \frac{2 \tan \frac{K_n}{2}}{1 + \tan^2 \frac{K_n}{2}}. \quad (3.41)$$

From the definition of discrete curvature, equation (3.41) is equivalent to equation (3.9) with $\alpha = 2(1 - \epsilon^2)/\Lambda^2$, which proves the second statement. \square

Remark 3.5. Proposition 3.4 provides discrete analogues for equations (2.7) and (2.15). In fact, by putting

$$\Lambda = 1 - \frac{h^2}{4}\lambda, \quad \epsilon = \frac{h^2}{4}\mu, \quad s = nh, \quad (3.42)$$

equations (3.30) and (3.31) yield equations (2.7) and (2.15) in the continuum limit $h \rightarrow 0$.

We next present explicit solutions for equation (3.30). Part of Proposition 3.6 and 3.8 can be found in [30], in a slightly different context: in that work, the function θ_n is regarded as the angle function (here denoted as Θ_n) instead of a potential function.

Proposition 3.6. The following functions satisfy equation (3.30):

(i)

$$\sin \frac{\theta_n}{2} = \operatorname{sn}(k^{-1}zn; k), \quad \operatorname{dn}(k^{-1}z; k) = \frac{1 - \epsilon}{1 + \epsilon}. \quad (3.43)$$

(ii)

$$\sin \frac{\theta_n}{2} = k \operatorname{sn}(zn; k), \quad \operatorname{cn}(z; k) = \frac{1 - \epsilon}{1 + \epsilon}. \quad (3.44)$$

Proof. For convenience, we write $u = k^{-1}zn$ and $v = k^{-1}z$. For (i), we show that equation (3.43) satisfies equation (3.31). Note that $\cos(\theta_n/2) = \operatorname{cn} u$ and $\cos(\theta_{n+1}/2) = \operatorname{cn}(u + v)$. Then, the right hand side of equation (3.31) is rewritten as

$$\begin{aligned} & \cos \left(\frac{\theta_{n+1} - \theta_n}{2} \right) + \epsilon \cos \left(\frac{\theta_{n+1} + \theta_n}{2} \right) = \frac{1}{1 - k^2 \operatorname{sn}^2 u \operatorname{sn}^2 v} \\ & \times \left[\left\{ (1 + \epsilon) \operatorname{cn}^2 u + (1 - \epsilon) \operatorname{sn}^2 u \operatorname{dn} v \right\} \operatorname{cn} v + \left\{ - (1 + \epsilon) \operatorname{dn} v + (1 + \epsilon) \right\} \operatorname{sn} u \operatorname{sn} v \operatorname{cn} u \operatorname{dn} v \right], \end{aligned} \quad (3.45)$$

where we used the addition formulas for the cn and sn functions. Imposing $\operatorname{dn} v = (1 + \epsilon)/(1 - \epsilon)$, we see that equation (3.31) is consistently reduced to $\Lambda = (1 + \epsilon) \operatorname{cn} v$. We prove (ii) in a similar manner. In fact, noticing that $\cos(\theta_n/2) = \operatorname{dn} u$ and imposing $\operatorname{cn} v = (1 + \epsilon)(1 - \epsilon)$, equation (3.31), with $u = zn$ and $v = z$, is consistently reduced to $\Lambda = (1 + \epsilon) \operatorname{dn} v$. \square

Remark 3.7.

(1) In case (i), the parameter α in equation (3.9) is given by

$$\alpha = 2 \frac{(1 - \epsilon^2)}{\Lambda^2} = 2 \frac{\operatorname{dn}(k^{-1}z; k)}{\operatorname{cn}^2(k^{-1}z; k)}, \quad (3.46)$$

which implies that θ_n in equation (3.43) corresponds to κ_n in equation (3.19). In case (ii),

$$\alpha = 2 \frac{(1 - \epsilon^2)}{\Lambda^2} = 2 \frac{\text{cn}(z; k)}{\text{dn}^2(z; k)}, \quad (3.47)$$

so that θ_n in equation (3.44) corresponds to κ_n in equation (3.20). These correspondences can be verified directly by computing κ_n from equations (3.43) and (3.44), respectively.

- (2) Continuum limits of equations (3.43) and (3.44) to equations (3.19) and (3.20), respectively, are obtained by putting $\epsilon = \frac{\mu}{4}h^2$ and taking the limit of $h \rightarrow 0$. This is consistent with Remark 3.3.

We finally present the variational formulation for equation (3.30).

Proposition 3.8 ([30], Sec. 2). Equation (3.30) is equivalent to the Euler-Lagrange equation of the functional

$$\tilde{S}_d = \sum_{n=0}^{N-1} \cos\left(\frac{\theta_{n+1} - \theta_n}{2}\right) - \epsilon \cos\left(\frac{\theta_{n+1} + \theta_n}{2}\right), \quad (3.48)$$

with respect to variations of the potential angle θ_n with fixed endpoints.

Proof. Let $L(\theta_n, \theta_{n+1}) = \cos((\theta_{n+1} - \theta_n)/2) - \epsilon \cos((\theta_{n+1} + \theta_n)/2)$. Then, the Euler-Lagrange equation is calculated as

$$\begin{aligned} 0 &= \frac{\partial}{\partial \theta_n} L(\theta_n, \theta_{n+1}) + \frac{\partial}{\partial \theta_n} L(\theta_{n-1}, \theta_n) \\ &= \cos\left(\frac{\theta_{n+1} - \theta_{n-1}}{4}\right) \left[\sin\left(\frac{\theta_{n+1} - 2\theta_n + \theta_{n-1}}{4}\right) + \epsilon \sin\left(\frac{\theta_{n+1} + 2\theta_n + \theta_{n-1}}{4}\right) \right], \end{aligned} \quad (3.49)$$

which gives equation (3.30). \square

Remark 3.9. Equation (3.30) can be seen as a reduction of two well known equations:

- (1) The discrete sine-Gordon equation [2, 10, 14],

$$\sin\left(\frac{\theta_{l+1}^{m+1} - \theta_l^{m+1} - \theta_{l+1}^m + \theta_l^m}{4}\right) = \frac{a}{b} \sin\left(\frac{\theta_{l+1}^{m+1} + \theta_l^{m+1} + \theta_{l+1}^m + \theta_l^m}{4}\right), \quad (3.50)$$

where a, b are lattice intervals. In fact, assuming that θ depends only on $n = l + m$, equation (3.50) is reduced to equation (3.30) with $\epsilon = -\frac{b}{a}$.

- (2) The discrete potential modified KdV equation [9],

$$\tan \frac{\theta_{l+1}^{m+1} - \theta_l^m}{4} = \frac{b+a}{b-a} \tan \frac{\theta_l^{m+1} - \theta_{l+1}^m}{4}, \quad (3.51)$$

or equivalently

$$\sin\left(\frac{\theta_{l+1}^{m+1} - \theta_l^{m+1} + \theta_{l+1}^m - \theta_l^m}{4}\right) = \frac{a}{b} \sin\left(\frac{\theta_{l+1}^{m+1} + \theta_l^{m+1} - \theta_{l+1}^m - \theta_l^m}{4}\right), \quad (3.52)$$

which describes the isoperimetric and equidistant deformation of discrete planar curves [13, 20], is transformed to the discrete sine-Gordon equation (3.50) by $\theta_l^m \rightarrow (-1)^m \theta_l^m$. In this sense, equation (3.30) can also be regarded as a reduction of the discrete potential modified KdV equation.

4 Approximation of discrete curves

In this section, we construct an algorithm to approximate a given discrete planar curve to a discrete elastica. Among the many possible discretizations for the elastica, the advantages of using the one shown in this work can be described as follows: First, the discrete elasticae are endowed with the same integrable structure as in their smooth counterpart, i.e., they possess several conserved quantities, can be obtained via a variational principle, and their explicit solutions are expressed in terms of Jacobi elliptic functions. Moreover, it is known that variational integrators have controlled error in their solutions [7, 18, 25]. In particular, the explicit expression for the discrete curvature κ_n is an “exact discretization” of the smooth curvature $\kappa(s)$ as discussed in Remark 3.3, and the potential function θ_n has the same functional shape as the smooth angle function $\theta(s)$. From these observations, we expect this discretization to have good numerical properties.

4.1 General discrete Euler’s elastica segment

To describe a general curve segment in the plane, we include the freedom of rotation in the equations. We do this by shifting the angle function and discrete angle function by a constant $\phi \in \mathbb{R}$ in all the expressions. In particular, equation (3.30) goes to

$$\sin\left(\frac{\theta_{n+1} - 2\theta_n + \theta_{n-1}}{4}\right) + \frac{\mu h^2}{4} \sin\left(\frac{\theta_{n+1} + 2\theta_n + \theta_{n-1}}{4} - \phi\right) = 0, \quad (4.1)$$

where we put $\epsilon = \mu h^2/4$, with $\mu > 0$ a constant. From Proposition 3.6, we have

$$(i) \quad \cos \frac{\theta_n - \phi}{2} = \text{cn}(k^{-1}(zn + q); k), \quad \sin \frac{\theta_n - \phi}{2} = \text{sn}(k^{-1}(zn + q); k), \quad (4.2)$$

$$(ii) \quad \cos \frac{\theta_n - \phi}{2} = \text{dn}(zn + q; k), \quad \sin \frac{\theta_n - \phi}{2} = k \text{sn}(zn + q; k), \quad (4.3)$$

where $k > 0$, $q, z \in \mathbb{R}$ are constants. The parameter k determines the shape of the elastica, q the initial point, and z is related with the length and point aggregation of the curve segment. Finally, from its starting point $\gamma_0 \in \mathbb{R}^2$, a discrete elastica segment is calculated recursively by

$$\gamma_n = \gamma_{n-1} + h \begin{bmatrix} \cos\left(\frac{\theta_{n+1}-\phi}{2} + \frac{\theta_n-\phi}{2} - \phi\right) \\ \sin\left(\frac{\theta_{n+1}-\phi}{2} + \frac{\theta_n-\phi}{2} - \phi\right) \end{bmatrix} \quad \text{for all } n = 1, \dots, N-1. \quad (4.4)$$

Note that we can expand the sine and cosine in equation (4.4) and make use of equation (4.3) to obtain an explicit expression in terms of the Jacobi elliptic functions. We conclude that a general discrete elastica segment can be characterized by seven parameters:

$$p = (x_0, y_0, h, \phi, z, q, k), \quad (4.5)$$

where $x_0, y_0 \in \mathbb{R}$ are the two components of the initial point γ_0 . We write as $\gamma_n(p)$ to the discrete elastica with parameters p .

4.2 Fairing process

Given a general discrete curve segment $\zeta_n \in \mathbb{R}^2$ ($n = 0, \dots, N-1$), we look for a discrete elastica $\gamma_n(p) \in \mathbb{R}^2$ that is the closest, in a L^2 -distance sense, to ζ_n . Namely, we seek to find p^* such that

$$p^* = \arg \min_{p \in U} \left\{ \sum_{n=0}^{N-1} \frac{1}{2} \|\gamma_n(p) - \zeta_n\|^2 \right\}, \quad (4.6)$$

where

$$U = \{(x_0, y_0, h, \phi, z, q, k) \mid x_0, y_0, \phi, z, q \in \mathbb{R} \wedge h, k > 0\}. \quad (4.7)$$

We solve this non-convex problem using the Interior Point Optimizer (IPOPT) package, that for our purpose can be seen as a gradient descent-like method for nonlinear optimizations [32]. For its implementation we need to compute the gradient and the Hessian of the objective function

$$\mathcal{L}(p) := \sum_{n=0}^{N-1} \frac{1}{2} \|\gamma_n(p) - \zeta_n\|^2. \quad (4.8)$$

For the gradient, we have

$$\frac{\partial}{\partial p_i} \mathcal{L}(p) = \sum_{n=0}^{N-1} \left\langle \gamma_n(p) - \zeta_n, \frac{\partial}{\partial p_i} \gamma_n(p) \right\rangle, \quad p_i = x_0, y_0, h, \phi, z, q, k, \quad (4.9)$$

which is computed recursively from equation (4.4),

$$\frac{\partial}{\partial p_i} \gamma_n(p) = \frac{\partial}{\partial p_i} \gamma_{n-1}(p) + \begin{cases} 0 & p_i = x_0, y_0, \\ T_n & p_i = h, \\ h \frac{\partial}{\partial p_i} T_n & \text{otherwise,} \end{cases} \quad \frac{\partial}{\partial p_i} \gamma_0 = \begin{cases} \begin{pmatrix} 1 \\ 0 \end{pmatrix} & p_i = x_0, \\ \begin{pmatrix} 0 \\ 1 \end{pmatrix} & p_i = y_0, \\ \begin{pmatrix} 0 \\ 0 \end{pmatrix} & \text{otherwise,} \end{cases} \quad (4.10)$$

Then, the only non-trivial derivatives we need to compute are

$$\frac{\partial}{\partial p_i} T_n = N_n \left(\frac{1}{C_{n+1}(p)} \frac{\partial}{\partial p_i} S_{n+1}(p) + \frac{1}{C_n(p)} \frac{\partial}{\partial p_i} S_n(p) \right), \quad p_i = z, q, k, \quad (4.11)$$

or equivalently,

$$\frac{\partial}{\partial p_i} T_n = -N_n \left(\frac{1}{S_{n+1}(p)} \frac{\partial}{\partial p_i} C_{n+1}(p) + \frac{1}{S_n(p)} \frac{\partial}{\partial p_i} C_n(p) \right), \quad p_i = z, q, k, \quad (4.12)$$

where we denoted $S_n \equiv \sin \frac{\theta_n - \phi}{2}$ and $C_n \equiv \cos \frac{\theta_n - \phi}{2}$. Finally, we use equations (4.2), (4.3) and the derivatives of the Jacobi elliptic functions with respect to their argument and module to complete the computation. For the Hessian, we use a numerical quasi-Newton approximation, internally computed by the package.

The IPOPT method needs a starting point \hat{p} , that we refer as the *initial guess*. In the following subsection we describe the algorithm that we use to obtain the initial guess, which is a discrete analogue of the one provided in [5].

4.3 Initial parameters

The initial guess, that starts the IPOPT method, can be obtained in a numerically stable manner thanks to two geometric properties of the discrete elastica: Proposition 4.1 and Corollary 4.1. Remarkably, these are geometrically equivalent to the same properties for the smooth elastica [5].

Let

$$\mathbf{I} = \begin{bmatrix} \sin \phi \\ -\cos \phi \end{bmatrix} \in \mathbb{R}^2, \quad (4.13)$$

and define the projection of the curve γ_n onto \mathbf{I} as

$$u_n = \langle \mathbf{I}, \gamma_n \rangle, \quad (4.14)$$

and the angle measured from \mathbf{I} as $\Psi_n = \frac{\pi}{2} + \Theta_n - \phi$ or, equivalently, such that

$$\begin{bmatrix} \cos \Psi_n \\ \sin \Psi_n \end{bmatrix} = R\left(\frac{\pi}{2} - \phi\right) T_n. \quad (4.15)$$

Proposition 4.1. *The discrete curvature κ_n is an affine function of the projection u_n , satisfying*

$$\kappa_n = \frac{\mu}{\Lambda} u_n + A, \quad (4.16)$$

where $\Lambda \in \mathbb{R}$ satisfies equation (3.31) and $A \in \mathbb{R}$ is a constant.

Proof. In the context of the proof of Proposition 3.4, after incorporating ϕ and putting $\epsilon = \mu h^2/4$, from equation (3.36) we obtain

$$\frac{\kappa_{n+1} - \kappa_n}{h} = -\frac{\mu}{\Lambda} \sin(\Psi_n - \phi). \quad (4.17)$$

Then, noticing that $u_{n+1} - u_n = h \langle \mathbf{I}, T_n \rangle$, we have

$$\frac{u_{n+1} - u_n}{h} = -\sin(\Psi_n - \phi). \quad (4.18)$$

Hence, by comparing equations (4.16) and (4.17), we conclude that there exists a constant $A \in \mathbb{R}$ such that, for all n ,

$$\kappa_n = \frac{\mu}{\Lambda} u_n + A. \quad (4.19)$$

□

Note that, by putting $\mu_1 = \mu \cos \phi$ and $\mu_2 = \mu \sin \phi$, equation (4.16) can be expressed as

$$\kappa_n = \frac{1}{\Lambda} (\mu_2 x_n - \mu_1 y_n) + A, \quad (4.20)$$

where $x_n, y_n \in \mathbb{R}$ are the two components of γ_n .

Corollary 4.2. *It holds that*

$$\sin \Psi_n = \frac{\mu}{2\Lambda} u_{n+1} u_n + A \frac{u_{n+1} + u_n}{2} + B, \quad (4.21)$$

where $B \in \mathbb{R}$ is a constant.

Proof. From the definition of u_n and Ψ_n in equations (4.14) and (4.15), respectively, we obtain

$$T_n = R(\phi) \begin{bmatrix} \sin \Psi_n \\ -\frac{u_{n+1}-u_n}{h} \end{bmatrix}, \quad N_n = R(\phi) \begin{bmatrix} \frac{u_{n+1}-u_n}{h} \\ \sin \Psi_n \end{bmatrix}. \quad (4.22)$$

Then, putting this into the discrete Frenet formula $(T_n - T_{n-1})/h = \kappa_n(N_n + N_{n-1})/2$ gives

$$\sin \Psi_n - \sin \Psi_{n-1} = \frac{1}{2} \left(\frac{\mu}{\Lambda} u_n + A \right) (u_{n+1} - u_{n-1}), \quad (4.23)$$

where we used (4.16). After expanding the right hand side of the previous expression and then adding $\pm \frac{A}{2} u_n$, we conclude that there exists a constant $B \in \mathbb{R}$ such that, for all n ,

$$\sin \Psi_n = \frac{\mu}{2\Lambda} u_{n+1} u_n + A \frac{u_{n+1} + u_n}{2} + B. \quad (4.24)$$

□

To estimate (ϕ, z, q, k) we use some results from the smooth elastica to avoid unnecessary complexity in the discrete case. We use the following approximations: From equation (3.31) with $\epsilon = \mu h^2/4$, taking equation (3.42) into account, equations (4.20) and (4.21) can be expanded in terms of $\sqrt{\mu}h$ as

$$\kappa_n = \mu_2 x_n - \mu_1 y_n + A + O(\mu h^2), \quad (4.25)$$

and

$$\sin \Psi_n = \frac{1}{2} \mu u_n^2 + A u_n + B + O(\mu h^2), \quad (4.26)$$

respectively. For the discrete curvature, note that solutions (3.19) and (3.20) can be written respectively as

$$\left\{ \begin{array}{l} \text{(i)} \quad \kappa_n = \kappa_{\max} \operatorname{dn}(k^{-1}(zn + q); k), \quad \kappa_{\max} = \frac{2}{h} \frac{\operatorname{sn}(k^{-1}z; k)}{\operatorname{cn}(k^{-1}z; k)}, \\ \text{(ii)} \quad \kappa_n = \kappa_{\max} \operatorname{cn}(zn + q; k), \quad \kappa_{\max} = \frac{2}{h} \frac{k \operatorname{sn}(z; k)}{\operatorname{dn}(z; k)}. \end{array} \right. \quad (4.27)$$

From Remark 3.7 we have $\alpha = 2 + \lambda h^2 + O(h^4)$, and it follows from equations (3.26) and (3.27) that $z = \sqrt{\mu}h + O(h^2)$. Then we can approximate κ_{\max} as

$$\left\{ \begin{array}{l} \text{(i)} \quad \kappa_{\max} = 2k^{-1} \sqrt{\mu} + O(\mu h^2), \\ \text{(ii)} \quad \kappa_{\max} = 2k \sqrt{\mu} + O(\mu h^2). \end{array} \right. \quad (4.28)$$

We obtain an approximation of the parameter k from these expressions. We see from equation (4.26) that u must be bound from above and below, the upper bound u_{\max} being

$$u_{\max} = \frac{-A + \Delta}{\mu} + O(h^2), \quad \Delta = \sqrt{A^2 - 2\mu(B - 1)}. \quad (4.29)$$

Noticing that u_{\max} occurs at the same instance as κ_{\max} , from equation (4.16) we have

$$\kappa_{\max} = \Delta + O(\mu h^2). \quad (4.30)$$

Hence, from equation (4.28) we obtain

$$\begin{cases} \text{(i)} & k = \frac{2\sqrt{\mu}}{\Delta} + O(\sqrt{\mu}h^2), \\ \text{(ii)} & k = \frac{\Delta}{2\sqrt{\mu}} + O(\sqrt{\mu}h^2). \end{cases} \quad (4.31)$$

Pseudo code: Given a discrete curve γ_n ($n = 0, 1, \dots, N - 1$) with segment length h , from their definition, we compute Θ_n such that

$$\Theta_n : \begin{bmatrix} \cos \Theta_n \\ \sin \Theta_n \end{bmatrix} = \frac{\gamma_{n+1} - \gamma_n}{h}, \quad \text{for all } n = 0, 1, \dots, N - 2, \quad (4.32)$$

and the discrete curvature κ_n by

$$\kappa_n := \frac{2}{h} \tan \frac{\Theta_n - \Theta_{n-1}}{2}, \quad \text{for all } n = 1, 2, \dots, N - 2. \quad (4.33)$$

Then, we obtain the initial guess $\hat{\rho}$ by solving equations (4.25) and (4.26) in the least-square sense and using several of the equations mentioned above. We proceed as follows:

- (parameter ϕ) From equation (4.25), compute

$$(\hat{\mu}_1, \hat{\mu}_2, \hat{A}) = \arg \min_{(\mu_1, \mu_2, A)} \left\{ \sum_{n=1}^{N-2} (\kappa_n + \mu_1 y_n - \mu_2 x_n - A)^2 \right\}, \quad (4.34)$$

then $\hat{\mu} = \sqrt{\hat{\mu}_1^2 + \hat{\mu}_2^2}$, and ϕ is such that $\cos \phi = \hat{\mu}_1 / \hat{\mu}$ and $\sin \phi = \hat{\mu}_2 / \hat{\mu}$.

- (parameter k) From equation (4.26), compute

$$\hat{B} = \arg \min_B \left\{ \sum_{n=0}^{N-2} \left(\sin \Psi_n - \frac{1}{2} \hat{\mu} u_n^2 - \hat{A} u_n - B \right)^2 \right\}. \quad (4.35)$$

From equation (4.31), if $\hat{B} < \frac{\hat{A}^2}{2\hat{\mu}} - 1$ we are in case (i) and

$$\hat{k} = 2 \left(\frac{\hat{A}^2}{\hat{\mu}} - 2(\hat{B} - 1) \right)^{-1/2}, \quad (4.36)$$

otherwise we are in case (ii) and

$$\hat{k} = \frac{1}{2} \left(\frac{\hat{A}^2}{\hat{\mu}} - 2(\hat{B} - 1) \right)^{1/2}. \quad (4.37)$$

- (parameter q and z) For simplicity, let $s_n = zn + q$. Define $m \in \mathbb{N}$ as the number of segments in which the function u_n is monotone. We counted m manually, although it could also be

estimated by, for example,

$$\begin{cases} \text{(i): } \hat{m} = \left[(N-1)h \frac{\sqrt{\hat{\mu}}}{K(\hat{k})} \right] (+1), \\ \text{(ii): } \hat{m} = \left[(N-1)h \frac{\sqrt{\hat{\mu}}}{2K(\hat{k})} \right] (+1), \end{cases} \quad (4.38)$$

where K is the complete elliptic integral of the first kind, and the term in brackets (+1) is added only if both u_0 and u_{N-1} are simultaneously increasing or decreasing. Now we can simply invert the Jacobi elliptic function at the endpoints $n = 0$ and $n = N - 1$ to obtain q and z . From equations (4.27) and (4.28), we have the following:

(i)

$$\text{dn}(\hat{k}^{-1}s_n; \hat{k}) = \frac{\hat{\mu}u_n + \hat{A}}{2\hat{k}^{-1}\sqrt{\hat{\mu}}} \quad (4.39)$$

which can be rewritten as

$$\text{sn}(\hat{k}^{-1}s_n; \hat{k}) = \hat{k}^{-1} \sqrt{1 - \left(\frac{\hat{\mu}u_n + \hat{A}}{2\hat{k}^{-1}\sqrt{\hat{\mu}}} \right)^2} \equiv U_n. \quad (4.40)$$

Hence,

– If u_n is decreasing on the first segment:

$$s_0 = \hat{k}F(\arcsin U_0; \hat{k}), \quad (4.41)$$

and

$$s_{N-1} = (m-1)\hat{k}K(\hat{k}) + \hat{k}F(\arcsin U_{N-1}; \hat{k}), \quad (4.42)$$

if m is odd, or

$$s_{N-1} = m\hat{k}K(\hat{k}) - \hat{k}F(\arcsin U_{N-1}; \hat{k}), \quad (4.43)$$

if m is even.

– If u_n is increasing on the first segment:

$$s_0 = 2\hat{k}K(\hat{k}) - \hat{k}F(\arcsin U_0; \hat{k}), \quad (4.44)$$

and

$$s_{N-1} = (m+1)\hat{k}K(\hat{k}) - \hat{k}F(\arcsin U_{N-1}; \hat{k}), \quad (4.45)$$

if m is odd, or

$$s_{N-1} = m\hat{k}K(\hat{k}) + \hat{k}F(\arcsin U_{N-1}; \hat{k}), \quad (4.46)$$

if m is even.

(ii)

$$\text{cn}(zn + q; \hat{k}) = \frac{\hat{\mu}u_n + \hat{A}}{2\hat{k}\sqrt{\hat{\mu}}} \equiv U_n. \quad (4.47)$$

Hence,

– If u_n is decreasing on the first segment:

$$s_0 = F(\arccos U_0; \hat{k}), \quad (4.48)$$

and

$$s_{N-1} = 2(m-1)K(\hat{k}) + F(\arccos U_{N-1}; \hat{k}), \quad (4.49)$$

if m is odd, or

$$s_{N-1} = 2mK(\hat{k}) - F(\arccos U_{N-1}; \hat{k}), \quad (4.50)$$

if m is even.

– If u_n is increasing on the first segment:

$$s_0 = 4K(\hat{k}) - F(\arccos U_0; \hat{k}), \quad (4.51)$$

and

$$s_{N-1} = 2(m+1)K(\hat{k}) - F(\arccos U_{N-1}; \hat{k}), \quad (4.52)$$

if m is odd, or

$$s_{N-1} = 2mK(\hat{k}) + F(\arccos U_{N-1}; \hat{k}), \quad (4.53)$$

if m is even.

Here we used the fact that $\text{sn}^{-1} = F \circ \arcsin$, $\text{cn}^{-1} = F \circ \arccos$, and F is the elliptic integral of the first kind. Finally,

$$\hat{q} = s_0, \quad \hat{z} = \frac{1}{N-1}(s_{N-1} - s_0). \quad (4.54)$$

- (parameters x_0 and y_0) From the previous steps, using all the recovered parameters, construct a discrete elastica segment that starts at the origin, $\hat{\gamma}$. Then,

$$(\hat{x}_0, \hat{y}_0) = \arg \min_{(x_0, y_0)} \left\{ \sum_{n=0}^{N-1} (\gamma_n - \hat{\gamma}_n)^2 \right\}. \quad (4.55)$$

Figure 5 illustrates typical examples of the fairing by the discrete elasticae obtained by using the above algorithm.

5 Application: characterization of keylines of Japanese hand-made pantiles

5.1 Background and outline

Sangawara (Japanese pantiles) are the most common type of roof tiles in Japan and are thought to be unique to the country. Although the number of buildings with sangawara roofs are decreasing, the landscapes with the remaining constructions having sangawara roofs are considered by the community to be one of the most beautiful scenes and culturally Japanese. Traditionally, sangawara were handmade from local clay by placing a clay plate on a wooden mold, beating it with a board

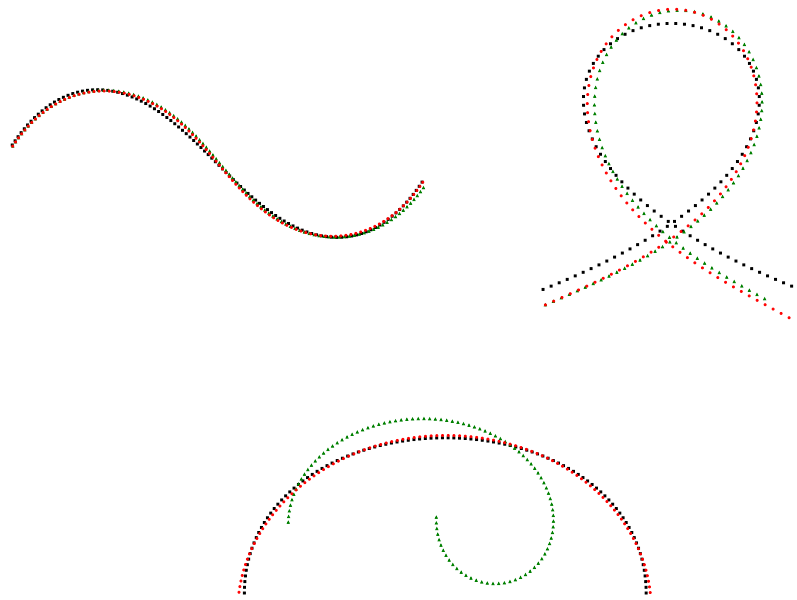


Figure 5: Typical examples of the fairing by the discrete elasticae. Black squares: input curve, green triangles: initial guess, red circles: output elastica.

called *tataki*, and stroking it with a board called *nadeita* (Figure 6). In recent times, they are mass-produced by metal mold presses in limited areas. The mold shapes are thought to be based on the shape of the sangawara in the handmade era, but companies keep their designs a trade secret, so it is not clear. We consider that it is important to characterize aesthetically pleasing curves like sangawara with mathematical formulas to be used in architectural design. Because of this, and the fact that the process involves bending the clay plate, we thought that the shape of sangawara could possibly be approximated by elasticae. In Section 5.2 we explain how the handmade sangawara (simply referred to as pantiles) were collected, in Section 5.3 we obtain the keyline of each pantile, and in Section 5.4 we approximate those keylines to discrete elasticae.



Figure 6: Beating (left) and stroking (right) in making handmade pantiles in demonstration class at Department of Architecture, Mukogawa Women's University.

5.2 Generation of 3D keyline data of pantiles

The pantiles we measured had been used in a house built around 1900 in Settsu City, Osaka Prefecture (Figure 7). From the characteristic shapes of the pantiles, they were likely used from the original construction or replaced before the revision of the urban building law in 1924 after the Great Kanto Earthquake. According to the owners, most of the tiles were blown away when the 2nd Muroto Typhoon hit in 1961, so they were collected and re-roofed. After that, only a few of the pantiles were replaced before the house was demolished in March 2017.

In our survey before the demolition, we found that the roofs of this house were covered by four different sizes of pantiles that ranged from 240 to 280 mm in working width. Prior to dismantling the building, we preserved six rows of pantiles (A to F in Figure 8) that covered those four sizes. The pantiles varied in shape due to their handmade nature, so we preserved six rows instead of only four individual pantiles. We measured 37 pantiles of the C and F with a working width of 270 mm (the most commonly used on this house), excluding the eave pantiles (C01, F01).



Figure 7: Exterior photos of house with pantile roofs.

We used the NextEngine’s Ultra HD 3D laser scanner and placed it and the pantiles as shown in Figure 9 for the measurements. The mesh data obtained from the 3D laser scanner was read by 3D Systems’ RapidWorks 64 4.1.0 reverse modeling software. We used this software to synthesize and decimate its polygons finer than the scanner’s measurement accuracy (0.3 mm) and then automatically heal incorrect data and fill holes in the meshes.

The two front edges are the 3D keylines of the pantile that could be observed when pitched. The lower edge could be generated by extracting the outer boundary curve of the mesh with RapidWorks. The upper edge could be generated by extracting the curve network from the mesh data with RapidWorks. Figure 10 shows an example of the two 3D keylines (upper and lower edges) generated. Each of these 3D keylines form an open polygon.

5.3 Generation and conversion of 2D keylines

Plane fitting of 3D keyline by principal component analysis

In order to generate 2D keyline data from the 3D keylines obtained from the scanning data, we need plane fitting of the 3D data. This can be done by projecting the points in \mathbb{R}^3 on the plane which minimizes the sum of squared distances from the points. As is well-known, such plane is constructed by applying the principal component analysis of the so-called the covariance matrix. More concretely, let $p_1, p_2, \dots, p_m \in \mathbb{R}^3$ be three-dimensional column vectors that represent spatial

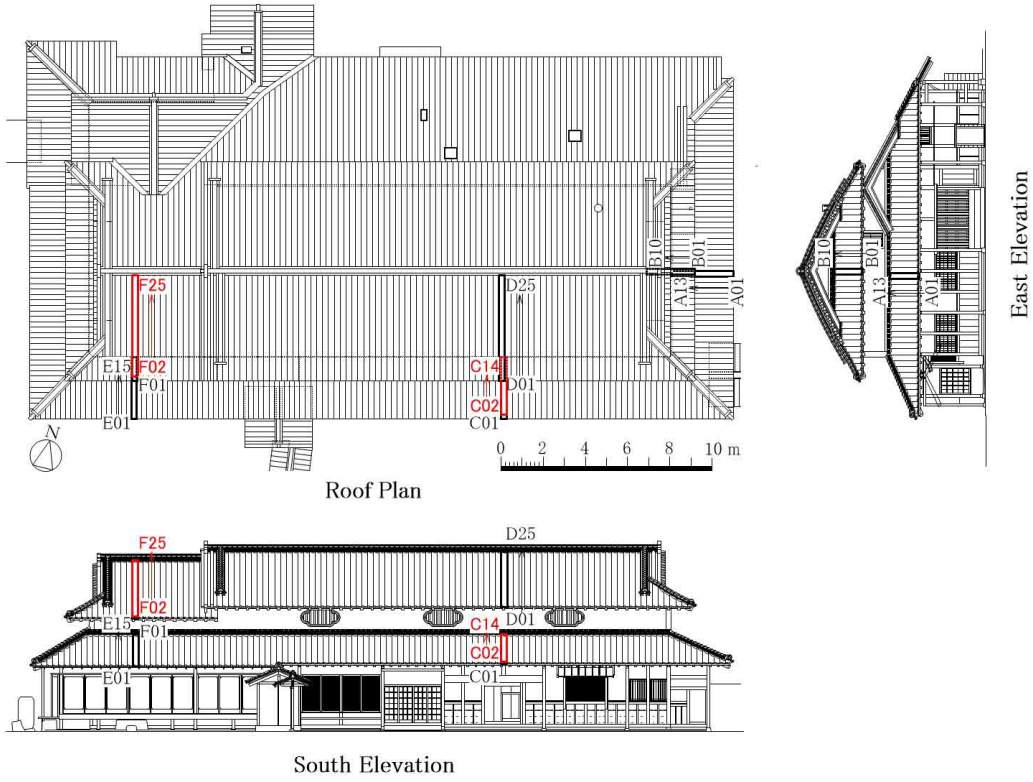


Figure 8: Preserved pantiles (black and red: A-F) and measured pantiles (red: C02-14, F02-25).

coordinates of a point cloud consisting of m points. Their center of gravity \bar{p} is given by

$$\bar{p} = \frac{1}{m} \sum_{k=1}^m p_k. \quad (5.1)$$

We consider the covariance matrix C defined by

$$C = \frac{1}{m} \sum_{k=1}^m (p_k - \bar{p}) {}^t(p_k - \bar{p}),$$

which is real, symmetric positive semi-definite matrix, and let e_1, e_2, e_3 be orthonormal eigenvectors that correspond to eigenvalues $\lambda_1, \lambda_2, \lambda_3$ ($\lambda_1 \geq \lambda_2 \geq \lambda_3 \geq 0$) of C . Then it is known that the plane π that includes \bar{p} and is parallel to e_1 and e_2 (i.e., with e_3 as the normal vector) minimizes the sum of the squared distances from p_1, p_2, \dots, p_m (see, for example, [1]). Therefore, plane fitting is obtained by projecting p_1, p_2, \dots, p_m onto π .

Following this idea, the xyz -coordinates of the point sequence consisting of all the vertices of the open polygon that constitutes one 3D skyline are converted into the $x'y'z'$ -coordinate system, where the center of gravity of the point sequence is the origin O' and the orientations of e_1, e_2 , and e_3 are the x', y' and z' axes, respectively. The orientations of e_1, e_2 , and e_3 are determined to be those of the x', y' and z' axes shown in Figure 9, respectively. When converting the coordinate p_k in the xyz -coordinate system into the coordinate p'_k in the $x'y'z'$ -coordinate system,

$$p'_k = {}^t(e_1 e_2 e_3)(p_k - \bar{p}),$$

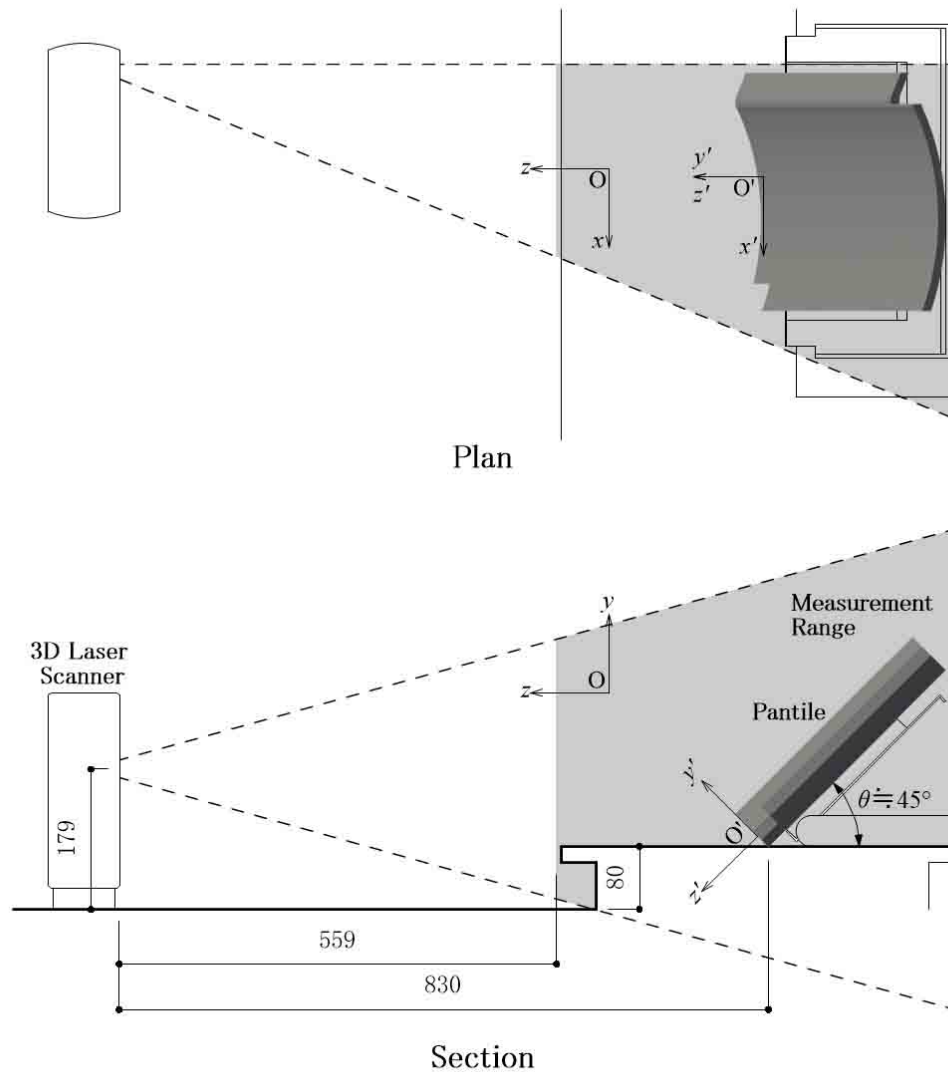


Figure 9: Placement of 3D laser scanner and pantile during measurement.

is satisfied because $(e_1 e_2 e_3)$ is an orthogonal matrix.

Equilateral open polygon approximation of 2D keyline

The 2D keylines obtained by projecting the 3D keylines onto the $x'y'$ planes in the previous paragraph (simply referred to as the 2D keylines before approximation) can be approximated by equilateral open polygons using the following procedure.

First, let the end point on the negative side of the x' axis of the 2D keyline before approximation (simply referred to as the left end) be the starting point A_1 after approximation, and let the point on the keyline whose distance from A_1 is r ($= 1.0$ mm) be A_2 . Next, let the point on the same keyline where the distance from A_2 is r and does not return to the left end (A_1) be A_3 . In the same way, repeat the operation to let the point whose distance from A_k is r and does not return to A_{k-1} be A_{k+1} (Figure 11). However, if there are multiple points that satisfy this condition, let the point on

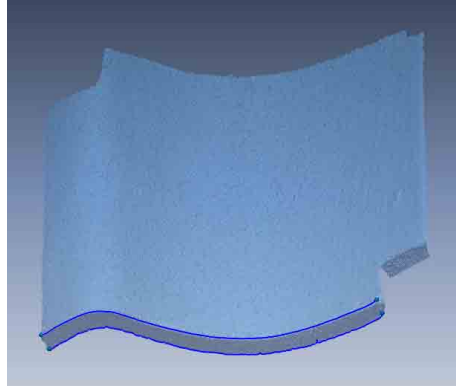


Figure 10: Example of 3D keylines generated (C07).

the keyline closer to the right end (the end point on the positive side of the x' axis) be A_{k+1} (Figure 12). When the only point that has a distance r from A_n is the point that returns to A_{n-1} , A_n is the stop point of the 2D keyline after approximation (Figure 13). All the points from the start point A_1 to the stop point A_n are connected on the sides to make the 2D keyline after approximation. The 2D keyline after approximation is an equilateral open polygon with n vertices, $n - 1$ sides, and $r(n - 1) = n - 1$ mm in total length.

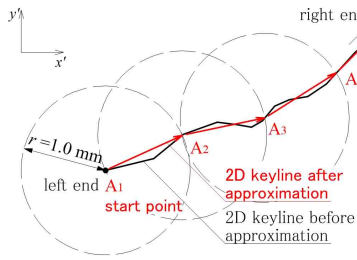


Figure 11: Procedure for equilateral open polygon approximation of 2D keyline (C07 lower keyline).

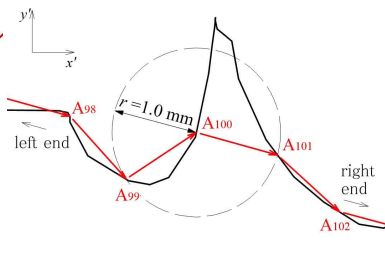


Figure 12: Method of determining vertex of equilateral open polygon when there are multiple points whose distance is r (C07 lower keyline).

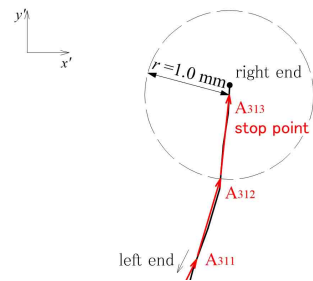


Figure 13: Method of determining stop point of equilateral open polygon (C07 lower keyline).

Coordinate conversion of 2D keylines after approximation by principal component analysis

When measuring the pantiles as shown in Figure 9, we place them one by one on the table by hand. Therefore, the position and rotation angle of each pantile is slightly different. To compare the curves of the keylines of the measured pantiles, we have to eliminate the effects of the positions and rotation angles and convert them into a coordinate system determined by only the keyline shape. This effect is already eliminated by conversion from the xyz -coordinate system into the $x'y'$ -coordinate system, where the center of gravity of the point sequence consisting of all the vertices of the 2D keyline is O' , the orientation of its first principal component is the x' axis,

and the orientation of its second principal component is the y' axis. However, the number and position of the points that compose the point sequence have been changed due to the equilateral open polygon approximation. Therefore, the center of gravity of the point sequence consisting of all vertices of the approximated 2D keyline does not generally coincide with O' , nor does the orientation of its first principal component coincide with the x' axis, nor does the orientation of its second principal component coincide with the y' axis. Because the relationship between the shape of the keyline and the coordinate system has been lost, the coordinate system must be converted again into one determined solely by the shape of the keyline. Therefore, by performing the principal component analysis again on the point sequence consisting of all the vertices of the 2D keyline after approximation, we convert the coordinates into the $x''y''$ -coordinate system with the center of gravity of the point sequence as O'' and the first principal component as the x'' axis. In the $x'y'$ -coordinate system, let q_1, q_2, \dots, q_n be the two-dimensional column vectors that represent the plane coordinates of the n points of the 2D keyline after approximation. Then their center of gravity \bar{q} is given by

$$\bar{q} = \frac{1}{n} \sum_{k=1}^n q_k.$$

Let f_1, f_2 be normalized eigenvectors that correspond to the eigenvalues μ_1, μ_2 ($\mu_1 \geq \mu_2$) of covariance matrix D defined by

$$D = \frac{1}{n} \sum_{k=1}^n (q_k - \bar{q}) {}^t(q_k - \bar{q}).$$

Here, the directions of f_1 and f_2 are determined so that the diagonal components of $(f_1 \ f_2)$ are all positive. When converting the coordinate q_k in the $x'y'$ -coordinate system into the coordinate q'_k in the $x'y'z'$ -coordinate system,

$$q'_k = {}^t(f_1 \ f_2)(q_k - \bar{q}),$$

is satisfied because $(f_1 \ f_2)$ is an orthogonal matrix.

In the following, the $x''y''$ -coordinates obtained by this coordinate conversion will be redefined as xy -coordinates.

Estimation of inflection point of approximate curve of 2D keyline

The approximate curve of the 2D keyline of the pantile has one global inflection point and is clearly asymmetric across the inflection point. In general, it is difficult to formulate such a curve in terms of a single elastica. Therefore, we estimate the global inflection point of the approximate curve, then we divide the curve on both sides of the inflection point and approximate them with different elastic curves. We estimate the inflection point using a method inspired by the Ramer-Douglas-Peucker (RDP) algorithm [6, 28], which was devised to simplify an open polygon with many vertices by thinning out the vertices (Figure 14). We call this the RDP method:

- (1) Among the vertices of the open polygon, let the point farthest from the line segment connecting the two end points be 3. Let the end point on the side with the inflection point (viewed from point 3) be 2, and let the end point on the side without the inflection point be 1.
- (2) Among the vertices of the open polygon between points 2 and 3, let the point farthest from line segment 2-3 be 4.

- (3) Among the vertices of the open polygon between the points P ($P = 3, 4, 5, \dots$) and $P + 1$, repeat the calculation to let the point farthest from the line segment $P(P + 1)$ be $P + 2$. However, the numbers of point P and point $P + 1$ are switched and the next calculation is performed if point $P + 1$ is the upper side of line segment $(P - 1)P$ and point $P + 2$ is also the upper side of line segment $P(P + 1)$, or, conversely, if point $P + 1$ is the lower side of line segment $(P - 1)P$ and point $P + 2$ is also the lower side of line segment $P(P + 1)$.
- (4) When points $P + 1$ and $P + 2$ become adjacent vertices on the open polygon, the calculation is terminated and the inflection point is estimated to be $P + 2$.

Because the RDP algorithm is intended to thin out the vertices, its calculation is terminated when an error falls within a certain range. However, the RDP method in this study is meant to estimate the inflection points. Therefore, we repeat the calculation only in the section where the inflection point is estimated to exist until it agrees with the original open polygon, and we estimate the converged point to be the inflection point.

5.4 Approximation of 2D keyline by discrete elastica

For the right (valley) sides of the inflection points of the 37 lower keylines (Figure 15) of the 37 pantiles, we tried to approximate the discrete elastica by the method already described. Among $p = (x_0, y_0, h, \phi, z, q, k)$ shown in (4.5), (x_0, y_0) were set as the inflection point to allow the discrete elastica to pass through the inflection point after approximation, and the remaining five parameters were optimized. An example of approximation of a keyline of a pantile (C07 lower keyline) by discrete elastica is shown in Figure 16, the calculation results of the 37 approximated discrete elasticae are shown in Figure 17, and the calculation results of the parameters h, ϕ, z, q, k are shown in Table 1.

Lower keylines right (valley) side	h [mm]	ϕ		z	q	k	
		[rad]	[grad]				
C02-14, F02-15, 17-23, 25	mean std. dev.	0.964 6.564×10^{-3}	-0.168 2.078×10^{-3}	-9.623 0.119	9.001×10^{-3} 1.263×10^{-3}	5.919 1.789×10^{-3}	0.353 1.235×10^{-2}
F16		0.945	2.045	117.192	67.36	5.226	27.43
F24		1.007	2.478	141.986	121.8	28.28	27.39

Table 1: Calculation results for h, ϕ, z, q and k (mean and standard deviation). Because the values for F16 and F24 were extremely different from the others, the means and standard deviations were calculated for the 35 keylines except for F16 and F24, and the values for F16 and F24 were written separately.

As Table 1 shows, the 35 key lines (except for F16 and F24) show very little variation in the calculated results of the parameters, and the discrete elasticae are similar in both shape and rotation angle. The k values are close to 0.3, and the shapes are close to sine curves. However, the values of ϕ, z, q and k for F16 and F24 are extremely different from the others. The k values exceed 10, and the shapes are close to arcs.

Figure 18 shows the 37 translated discrete elasticae shown in Figure 17 with the inflection point (x_0, y_0) at the origin. The variations of the discrete elasticae are larger than that in Figure 17, suggesting that a certain number of variations and errors may be included in the estimations of the

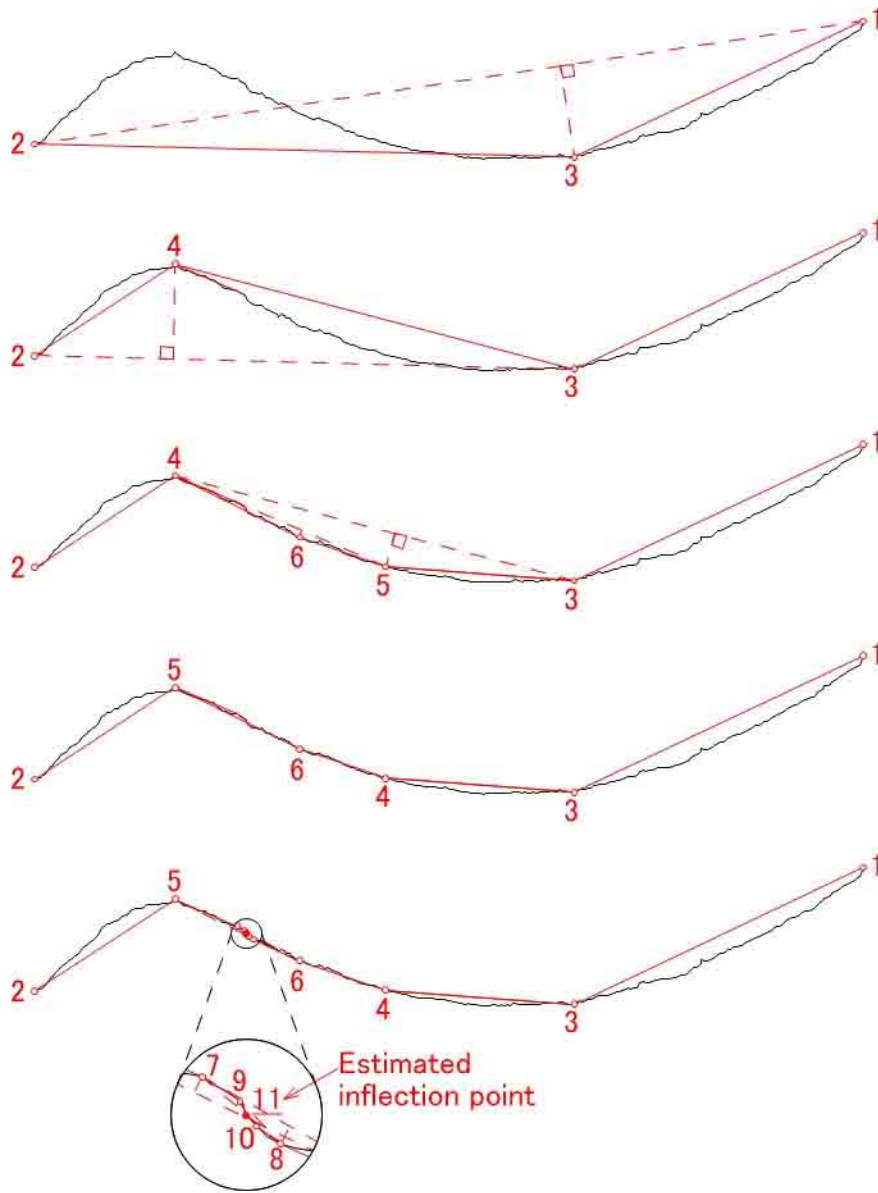


Figure 14: Example of inflection point estimation by RDP method (C07 lower keyline). In the first three curves we apply steps (1), (2) and (3), respectively. In the fourth and fifth curves, following step (3), we switch point 4 to point 5, and point 7 to point 11, respectively. Finally, in the augmented image at the bottom, following step (4), the inflection point is estimated to be point 11.

inflection points. In F16 and F24 in particular, the estimated inflection points are located closer to the right (valley) sides. Therefore, we can assume that the areas around the inflection points where the curvature is small are largely omitted, and the discrete elasticae are approximated to be close to the arcs. The effect the local unevenness of the keyline has on the estimation of the inflection point should be examined. In conclusion, we found that 35 of the 37 lower keylines of the handmade pantiles could be approximated by discrete elasticae with a very small variation on the right (valley)

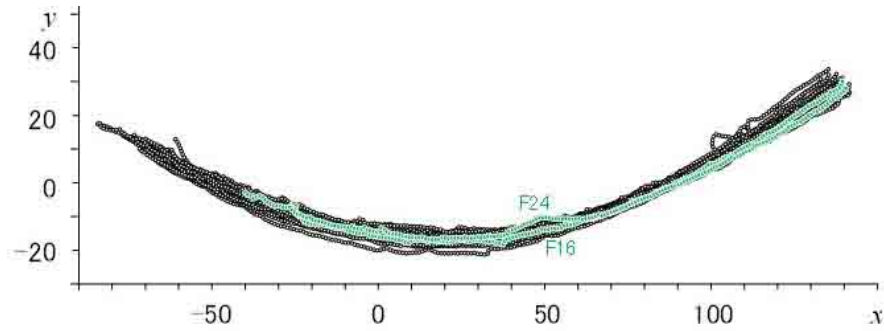


Figure 15: Right (valley) sides of 2D lower keylines for calculation.

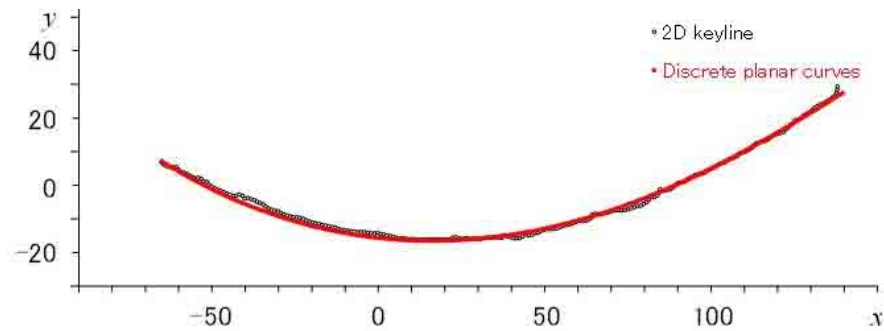


Figure 16: Example approximation by discrete elastica (C07 lower keyline).

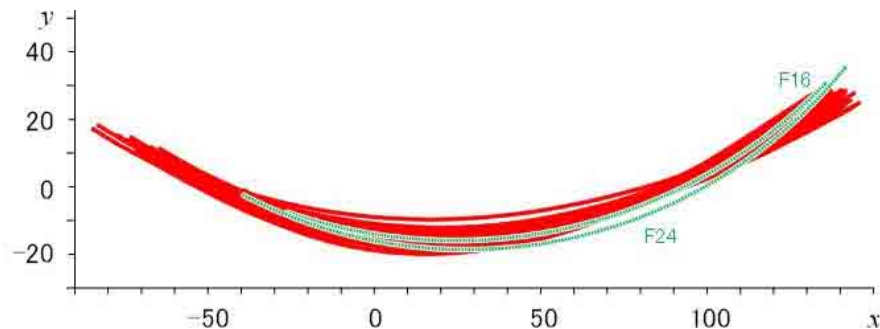


Figure 17: Calculation results of approximated discrete elasticae of 2D lower keylines.

side of the inflection point. However, the errors of the estimated positions of the inflection points may affect the accuracy of the approximations.

Acknowledgements

The authors would like to thank Professor David Brander for encouragement. They also express their thanks to Professors Nozomu Matsuura, Jun-ichi Inoguchi, Kenjiro T. Miura, Satoshi Kanai and Dr. Masahisa Asada for fruitful discussions. They would like to thank Mr. Konosuke Onishi, Mr. Yunosuke Onishi, Associate Professor Toshikazu Inoue, and Mr. Daisuke Mitsumoto for their cooperation in the housing survey. This work was initiated by the 2018 IMI Joint Use Research

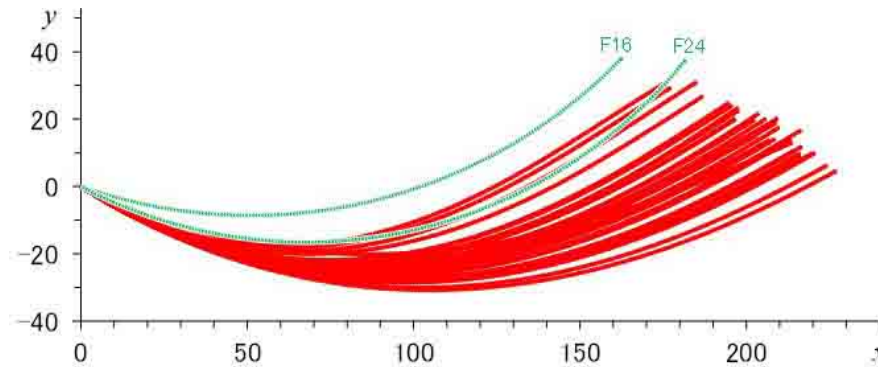


Figure 18: Result of translating discrete elasticae in Figure 17 so that each inflection point is at origin. Calculation results of F16 and F24 are clearly quite different from others.

Program Short-Term Joint Research No.20180008, and supported by JSPS Kakenhi JP16H03941, 17K00741, 20K12520, 21K03329 and JST CREST Grant Number JPMJCR1911.

References

- [1] J. Berkmann and T. Caelli, Computation of surface geometry and segmentation using covariance techniques, *IEEE PAMI* **16**(1994) 1114–1116.
- [2] A. Bobenko and U. Pinkall, Discrete surface with constant negative Gaussian curvature and the Hirota equation, *J. Differential Geom.* **43** (1996) 527–611.
- [3] A. I. Bobenko, Yu. B. Suris, Discrete Time Lagrangian Mechanics on Lie Groups, with an Application to the Lagrange Top, *Commun. Math. Phys.* **204**(1999) 147–188.
- [4] A. Bobenko, *Geometry II – Discrete Differential Geometry* (May 31, 2007), available at: [http://page.math.tu-berlin.de/~techter/lecture notes/geometry2 lecture notes.pdf](http://page.math.tu-berlin.de/~techter/lecture%20notes/geometry2%20lecture%20notes.pdf)
- [5] D. Brander, J. Gravesen and T. B. Nørbjerg, Approximation by planar elastic curves, *Adv. Comput. Math.* **43**(2017) 25–43.
- [6] D. Douglas and T. Peucker, Algorithms for the reduction of the number of points required to represent a digitized line or its caricature, *The Canadian Cartographer* **10** (1973) 112–122.
- [7] J. Fernández, S. Graiff Zurita and S. Grillo, Error analysis of forced discrete mechanical systems, Manuscript submitted to *AIMS' Journals* (2020)
- [8] R.E. Goldstein and D.M. Petrich, The Korteweg-de Vries hierarchy as dynamics of closed curves in the plane, *Phys. Rev. Lett.* **67** (1991) 3203–3206.
- [9] R. Hirota, Discretization of the potential modified KdV equation, *J. Phys. Soc. Jpn.* **67** (1998) 2234–2236.
- [10] R. Hirota, Nonlinear partial difference equations. III. Discrete sine-Gordon equation, *J. Phys. Soc. Jpn.* **43**(1977) 2079–2086.

- [11] T. Hoffmann and N. Kutz, Discrete Curves in \mathbb{CP}^1 and the Toda Lattice, *Stud. in Appl. Math.* **113**(2004) 31–55.
- [12] T. Hoffmann, Discrete Differential Geometry of Curves and Surfaces, *MI Lecture Notes* **18** (Kyushu University, Fukuoka, 2009).
- [13] J. Inoguchi, K. Kajiwara, N. Matsuura and Y. Ohta, Motion and Bäcklund transformations of discrete planar curves, *Kyushu J. Math.* **66**(2012) 303–324.
- [14] J. Inoguchi, K. Kajiwara, N. Matsuura and Y. Ohta, Discrete mKdV and discrete sine-Gordon flows on discrete space curves. *J. Phys. A: Math. Theoret.* **47**(2014) 235202.
- [15] K. Kajiwara, Y. Ohta, J. Satsuma, B. Grammaticos and A. Ramani, Casorati determinant solutions for the discrete Painlevé-II equation, *J. Phys. A: Math. Gen.* **27**(1994) 915–922.
- [16] K. Kajiwara, M. Noumi and Y. Yamada, Geometric Aspects of Painlevé equations, *J. Phys. A: Math. Theor.* **50** (2017) 073001 (164pp).
- [17] D. F. Lawden, Elliptic Functions and Applications, *Applied Mathematical Sciences*, vol. 80. Springer-Verlag, New York (1989)
- [18] J. E. Marsden and T. S. Ratiu, Introduction to mechanics and symmetry, Second ed., *Texts in Applied Mathematics*, vol. 17 (Springer-Verlag, New York, 1999).
- [19] S. Matsutani, S. Euler’s Elastica and Beyond. *J. Geom. Symmetry Phys.* **17** (2010) 45–86.
- [20] N. Matsuura, Discrete KdV and discrete modified KdV equations arising from motions of planar discrete curves, *Int. Math. Res. Notices*, **43** (2011) rnn080 (18 pages).
- [21] N. Matsuura, An explicit formula for discrete planar elastic curves, a talk given at the Annual Meeting of Mathematical Society of Japan (March 18, 2020) (in Japanese).
- [22] E.M. McMillan, Some thoughts on stability in nonlinear periodic focusing systems, UCRL-17795 (1967). Available at: <https://escholarship.org/uc/item/8zq4t2pc>
- [23] D. Mumford, Elastica and computer vision, *Algebraic Geometry and Its Applications* (West Lafayette, IN, 1990), (Springer, New York, 1994) pp. 491–506.
- [24] NIST Digital Library of Mathematical Functions, <https://dlmf.nist.gov/> .
- [25] G. W. Patrick, C. Cuell, Error analysis of variational integrators of unconstrained Lagrangian systems, *Numer. Math.* **113** (2009) 243—264.
- [26] G.R.W. Quispel, J.A.G. Roberts and C.J. Thompson, Integrable mappings and soliton equations, *Phys. Lett.* **A126**(1988) 419–421.
- [27] A. Ramani, B. Grammaticos, and J. Hietarinta, Discrete versions of the Painlevé equations, *Phys. Rev. Lett.* **67**(1991) 1829–1832.
- [28] U. Ramer, An iterative procedure for the polygonal approximation of plane curves, *Comput. Graph. Image Process.* **1** (1972) 244–256.

- [29] David A. Singer, Lectures on elastic curves and rods, Curvature and variational modeling in physics and biophysics, AIP Conf. Proc. **1002** (2008) 3–32.
- [30] K. Sogo, Variational discretization of Euler’s elastica problem, J. Phys. Soc. Jpn. **75** (2006) 064007.
- [31] D. Takahashi, T. Tokihiro, B. Grammaticos, Y. Ohta and A. Ramani, Constructing solutions to the ultradiscrete Painlevé equations J. Phys. A: Math. Gen. **30** (1997) 7953–7966.
- [32] A. Wächter and L.T. Biegler, On the implementation of an interior-point filter line-search algorithm for large-scale nonlinear programming, Math. Program., Ser. A **106** (2006) 25–57.